Eur. Phys. J. Plus (2017) **132**: 470
DOI 10.1140/epjp/i2017-11737-8

THE EUROPEAN PHYSICAL JOURNAL PLUS

Regular Article

Modelling and analysis of transient state during improved coupling procedure with the grid for DFIG based wind turbine generator

Soulaymen Kammoun[a], Souhir Sallem[b], and Mohamed Ben Ali Kammoun[c]

Commande de Machines Electriques et Réseaux de Puissance (CMERP), National Engineering School of Sfax, University of Sfax, Sfax, Tunisia

Received: 11 April 2016 / Revised: 2 October 2017
Published online: 9 November 2017 –

Abstract. The aim of this study is to enhance DFIG based Wind Energy Conversion Systems (WECS) dynamics during grid coupling. In this paper, a system modelling and a starting/coupling procedure for this generator to the grid are proposed. The proposed non-linear system is a variable structure system (VSS) and has two different states, before and after coupling. So, two different state models are given to the system to analyse transient stability during the coupling. The given model represents well the transient state of the machine, through which, a behaviour assessment of the generator before, during and after connection is given based on simulation results. For this, a 300 kW DFIG based wind generation system model was simulated on the `Matlab/SIMULINK` environment. We judge the proposed procedure to be practical, smooth and stability improved.

1 Introduction

Environmental concerns about global warming, and exhausting fossil fuels are the reason behind renewable energy sources emerging so to fulfil society's energy demand. Among all the renewable energy sources, wind energy is becoming mainstream and competitive with conventional sources of energy. The capacity of cumulative installed wind power increased from 6.1 GW in 1996 to 486.8 GW by 2016. It is predicted, following this trend, that the cumulative wind capacity would reach 800 GW by the end of 2021. More than 54 GWs of clean renewable wind power, for example, was added across the global market in 2016 [1–4].

This exponential growth in wind turbines plants had surely led to growing requirements in wind energy technology for better controlling the turbine as well as modelling the wind system. Most of the challenges in the wind power technology come from the fluctuating nature of wind flow applied to wind turbines. It can be noted that if newer technologies can overcome most annoying challenges in the future, a big part of the world's electricity demand can be provided only by wind energy [3]. Mainly, the aim of wind turbine systems development is to continuously increase output power. Modern high-power wind turbines are capable of Adjustable Speed Operation to overcome several drawbacks which were found on fixed speed generators. Many topologies based on different types of generators have then been proposed, and recent developments seek to avoid most of their disadvantages like the full-seized converters and filters in the case of synchronous generators.

Among adjustable speed generator, Doubly Fed Induction Generators (DFIGs) based wind turbines have become popular due to their numerous advantages including lower converters size and cost, variable speed operation at constant stator frequency, higher efficiency and independent control of both active and reactive powers.

Power control of the machine (MPPT and active/reactive power control) was the subject of recent researches. The grid is modelled as a stable and balanced voltage in most of the conventional control schemes [5–8]. However, many researchers have tried to propose new control schemes addressed to unbalanced networks to overcome such unfavourable conditions [9–12].

Another important axis of research related to the DFIG based WECS, is the rotor EMF, FACTS devices (such as STATCOM and SVC) and Energy Storage System (ESS) improvements in DFIG for Low Voltage Ride

[a] e-mail: `soulaymen.kammoun@gmail.com`
[b] e-mail: `souhirsallem@gmail.com`
[c] e-mail: `mbakammoun@gmail.com`

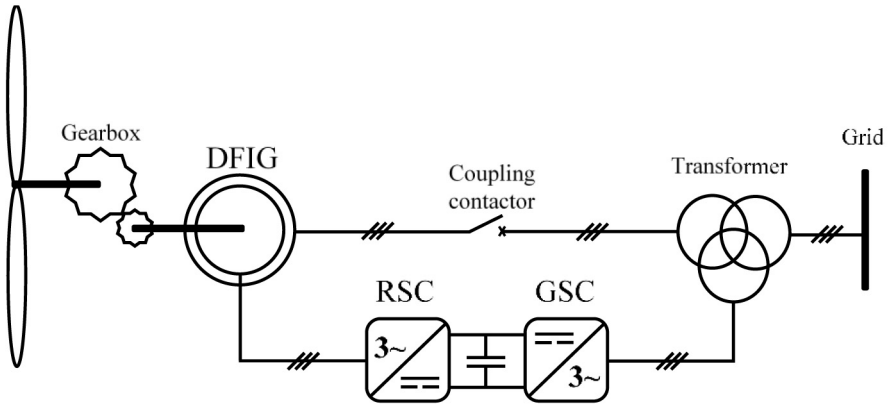

Fig. 1. Schematic diagram of a doubly fed induction generator based wind turbine.

Through (LVRT) purposes. For example, in [13] and [14], it was proven that by means of FACTS devices used in wind farms, instability caused by load voltage bus fluctuation was healed within a short time. It was also found in [15] that in the DFIG model the system became stable in a short time when using the Demagnetization Current Controller (DCC). Two detailed investigations were made in [16] and [17] of transient events, respectively, with and without active LVRT capability and with and without non-linear–type supercapacitor Energy Storage System (ESS), and it was found that the system became stable quickly when those devices (Active LVRT / Supercapacitor ESS) were incorporated into the reduced order DFIG model. So far, power control in DFIG wind generation systems either for balanced or unbalanced conditions is deeply investigated.

Although the control of variable speed wind turbines is an important area and obviously widely developed by researchers and manufacturers, there is not much to be found in the available literature about practical solutions or how manufacturers are doing to connect DFIG based wind turbine to the grid [18–20]. Most of the research papers are dealing with post-coupling problems.

As the utility grid is susceptible for several types of fault, the wind turbine is likely also to be disconnected and reconnected to the grid, and this, may be a few times per day. This explains our interest in this study of modelling transient state during connection. There are so far two techniques for connecting a DFIG to the grid published. The first technique relies on Direct Torque Control (DTC) [18], the second one relies on Field-Oriented Control (FOC) [19]. Although the simplicity of these techniques, they cannot guarantee a connection without a considerable impact to the grid and/or the machine. High inrush currents may happen during connection if sudden parameters variation occurs. Based also on FOC control, a synchronization algorithm is proposed in [20] as an improvement of [19]. The d-axis current is controlled, so the stator EMF amplitude, frequency and phase angle concords with grid voltage. This technique leads sometimes to some instabilities and especially rotor shaft stress with severe parameters variations.

In this paper, DFIG rotor windings are supplied (excitation) in a way to have a stator EMF synchronised with the grid voltage in a simple way without automated control (but it could be), to keep it simple and understandable. A simple values calculator computes corresponding values of frequency, amplitude and phase angle that make the stator EMF synchronized with grid voltage. Furthermore, the generator is connected to the grid when the mechanical torque is zero (so be the mechanical power), which prevents mechanical stress on the rotor shaft during the connection as there is no power transmission between the grid and the generator.

Remainder of the work is divided into four sections. In sect. 2, the modelling and dynamics of the system components are given. Section 3 deals with starting/coupling strategy steps using the new approach. Section 4 is devoted to simulation of results and discussion. The last section of this work presents the conclusions.

2 Dynamics and modelling of the wind generation system

The topology of the generator under study is given in fig. 1. The rotor of the turbine is coupled to the doubly fed induction generator through a gearbox. The electric generator is coupled to the grid system directly from the stator side and through a bidirectional back-to-back power converter from the rotor side.

2.1 Wind turbine model

The mechanical torque extracted from the wind on the DFIG shaft is given by applying the actuator disk theory [21]:

$$T_m = P_m \times \frac{1}{\omega_m}\,, \tag{1}$$

where ω_m (rad/s) is the DFIG's mechanical rotor angular speed and P_m (W) is the mechanical power. P_m is a function of the conversion ratio, the turbine's characteristics and the wind speed. It is given by

$$P_m = \frac{1}{2} C_p \rho \pi R^2 v_{\text{wind}}^3, \tag{2}$$

where $C_p(\lambda, \beta)$ is the power coefficient (Betz coefficient), ρ (Kg/m^3) is the air density, R (m) is the rotor disk radius and v_{wind} (m/s) is the wind speed. Several models exist in literature for the power coefficient [22]. The model given by eq. (3) will be considered as the most used and well adapted for variable speed wind turbines,

$$C_p(\lambda, \beta) = 0.5176 \left(\frac{116}{\lambda_i} - 0.4\beta - 5 \right) e^{-\frac{21}{\lambda_i}} + 0.0068\lambda, \tag{3}$$

where β is the blades pitch angle, λ is the tip speed ratio (given by eq. (4)) and $\lambda_i(\lambda, \beta)$ is given by (5):

$$\lambda = \frac{\omega \cdot R}{v_{\text{wind}}} = \frac{\omega_m \cdot R}{G \cdot v_{\text{wind}}}, \tag{4}$$

where ω is the turbine's angular speed (rad/s) and G is the gearbox ratio,

$$\frac{1}{\lambda_i} = \frac{1}{\lambda + 0.08\,\beta} - \frac{0.035}{\beta^3 + 1}. \tag{5}$$

2.2 Generator model under loaded conditions

The DFIG can be modelled in grid-connected operation (loaded DFIG) in a synchronous reference frame by eqs. (6) to (11) [23,24]. "d" and "q" subscripts represent, respectively, direct and quadrature components of the vector $\overline{x}$ ($\overline{x} = X_d + iX_q$).

Electrical equations

Equations for stator windings are as follows:

$$\begin{cases} V_{sd} = R_s I_{sd} + \dot{\psi}_{sd} - \omega_1 \psi_{sq}, \\ V_{sq} = R_s I_{sq} + \dot{\psi}_{sq} + \omega_1 \psi_{sd}, \end{cases} \tag{6}$$

$$\begin{cases} \psi_{sd} = L_s I_{sd} + M I_{rd}, \\ \psi_{sq} = L_s I_{sq} + M I_{rq}, \end{cases} \tag{7}$$

where $V_{s(dq)}$ are the stator voltages, $I_{s(dq)}$ are stator currents, $\psi_{s(dq)}$ are the stator flux, ω_1 is the stator current pulsation, R_s and L_s are, respectively, the stator resistance and inductance and $M = \frac{2}{3} m_{sr}$, m_{sr} is the maximum inductance value between a stator phase and a rotor phase.

For rotor windings:

$$\begin{cases} V_{rd} = R_r I_{rd} + \dot{\psi}_{rd} - (\omega_1 - \omega_r)\psi_{rq}, \\ V_{rq} = R_r I_{rq} + \dot{\psi}_{rq} + (\omega_1 - \omega_r)\psi_{rd}, \end{cases} \tag{8}$$

$$\begin{cases} \psi_{rd} = L_r I_{rd} + M I_{sd}, \\ \psi_{rq} = L_r I_{rq} + M I_{sq}, \end{cases} \tag{9}$$

where $V_{r(dq)}$ are the rotor voltages, $I_{r(dq)}$ are the rotor currents, $\psi_{r(dq)}$ are the rotor flux, ω_r is the rotor speed in electrical coordinates ($\omega_r = p\omega_m$, p is number of pole pairs), R_r and L_r are, respectively, the rotor resistance and inductance.

The electromagnetic torque is

$$T_{em} = \frac{3}{2} p \frac{M}{L_s} \left(I_{rd}\psi_{sq} - I_{rq}\psi_{sd} \right). \tag{10}$$

Mechanical equation

Neglecting the friction effect on the rotor which affects the mechanical equation (11) only for small size machines, the equation becomes as follows:

$$\frac{\mathrm{d}\omega_r}{\mathrm{d}t} = \frac{p}{J}(T_m - T_{em}). \tag{11}$$

2.3 Generator model under unloaded conditions

An unloaded DFIG do not have exactly the same behaviour or dynamic with a loaded one. We have to take into consideration that there are no stator currents as it is decoupled from the grid, but still, flux exists. The new equations are given by eqs. (12) to (17).

Electrical equations

As the generator is decoupled from the grid, and there is no voltage drop in the stator due to its resistance, there is an EMF in stator terminals instead of a voltage that will be noted e_s.

For stator windings:

$$\begin{cases} E_{sd} = -\dot{\psi}_{sd} + \omega_1 \psi_{sq}, \\ E_{sq} = -\dot{\psi}_{sq} - \omega_1 \psi_{sd}, \end{cases} \tag{12}$$

$$\begin{cases} \psi_{sd} = M I_{rd}, \\ \psi_{sq} = M I_{rq}. \end{cases} \tag{13}$$

For rotor windings:

$$\begin{cases} V_{rd} = R_r I_{rd} + \dot{\psi}_{rd} - (\omega_1 - \omega_r)\psi_{rq}, \\ V_{rq} = R_r I_{rq} + \dot{\psi}_{rq} + (\omega_1 - \omega_r)\psi_{rd}, \end{cases} \tag{14}$$

$$\begin{cases} \psi_{rd} = L_r I_{rd} + M I_{sd}, \\ \psi_{rq} = L_r I_{rq} + M I_{sq}. \end{cases} \tag{15}$$

The electromagnetic torque:

$$T_{em} = 0. \tag{16}$$

Mechanical equation

As the electromagnetic torque is zero, the rotational speed dynamics becomes

$$\frac{\mathrm{d}\omega_r}{\mathrm{d}t} = \frac{p}{J} T_m. \tag{17}$$

2.4 VSS modelling of the grid connected DFIG

Writing the above electrical loaded model into matrix mode gives

$$[\dot{\Psi}] = [\mathbb{R}_l][\mathbb{I}] + [\Omega_l][\Psi] + [\mathbb{V}_l], \tag{18}$$

with

$$[\Psi] = [\psi_{sd}\ \psi_{sq}\ \psi_{rd}\ \psi_{rq}]^T = [\mathbb{L}_l][\mathbb{I}], \qquad [\mathbb{V}_l] = [-V_{sd}\ -V_{sq}\ V_{rd}\ V_{rq}]^T, \qquad [\mathbb{I}] = [I_{sd}\ I_{sq}\ I_{rd}\ I_{rq}]^T,$$

$$[\mathbb{R}_l] = \begin{bmatrix} R_s & 0 & 0 & 0 \\ 0 & -R_s & 0 & 0 \\ 0 & 0 & R_r & 0 \\ 0 & 0 & 0 & R_r \end{bmatrix}, \qquad [\mathbb{L}_l] = \begin{bmatrix} L_s & 0 & M & 0 \\ 0 & L_s & 0 & M \\ M & 0 & L_r & 0 \\ 0 & M & 0 & L_r \end{bmatrix} \quad \text{and} \quad [\Omega_l] = \begin{bmatrix} 0 & \omega_1 & 0 & 0 \\ -\omega_1 & 0 & 0 & 0 \\ 0 & 0 & \omega_r - \omega_1 & 0 \\ 0 & 0 & 0 & \omega_1 - \omega_r \end{bmatrix}.$$

As $[\mathbb{L}_l]$ is a square matrix and its determinant is not zero, we can write also

$$[\dot{\Psi}] = [\mathbb{R}_l][\mathbb{L}_l]^{-1}[\Psi] + [\Omega_l][\Psi] + [\mathbb{V}_l], \tag{19}$$

$$[\dot{\Psi}] = [A_l][\Psi] + [\mathbb{V}_l], \tag{20}$$

with $[A_l] = [\mathbb{R}_l][\mathbb{L}_l]^{-1} + [\Omega_l]$.

For the unloaded model, rearranging eqs. (12) to (15) into matrix form gives

$$[\dot{\Psi}] = [\mathbb{R}_u][\mathbb{L}_{u-1}][\Psi] + [\Omega_u][\Psi] + [\mathbb{V}_u], \tag{21}$$

with

$$[\Omega_u] = [\Omega_l], [\mathbb{V}_u] = [-E_{sd} \ -E_{sq} \ V_{rd} \ V_{rq}]^T,$$

$$[\mathbb{R}_u] = \begin{bmatrix} 0 & 0 & 0 & 0 \\ 0 & 0 & 0 & 0 \\ 0 & 0 & R_r & 0 \\ 0 & 0 & 0 & R_r \end{bmatrix} \quad \text{and} \quad [\mathbb{L}_{u-1}] = \begin{bmatrix} 0 & 0 & 0 & 0 \\ 0 & 0 & 0 & 0 \\ 0 & 0 & 1/L_r & 0 \\ 0 & 0 & 0 & 1/L_r \end{bmatrix}.$$

We note $[\mathbb{L}_{u-1}]$ instead of $[\mathbb{L}_u]^{-1}$ as there is no invertible $[\mathbb{L}_u]$ matrix. An invertible $[\mathbb{L}_u]$ matrix does not exist as there are no stator currents and flux are only function of rotor currents.

Finally,

$$[\dot{\Psi}] = [A_u][\Psi] + [\mathbb{V}_u], \tag{22}$$

with $[A_u] = [\mathbb{R}_u][\mathbb{L}_{u-1}] + [\Omega_u]$.

To compile a single dynamic model, a trigger is inserted designing the coupling moment. This trigger is a Boolean variable and represents in reality the coupling contactor. The combined model of the DFIG is then given by eqs. (23) and (24):

$$[\dot{\Psi}] = (([A_l] - [A_u])\,\mathrm{trig} + [A_u])\,[\Psi] + (([V_l] - [V_u])\,\mathrm{trig} + [V_u])\,, \tag{23}$$

$$\frac{\mathrm{d}\omega_r}{\mathrm{d}t} = \frac{p}{J}(T_m - \mathrm{trig} \cdot T_{em}), \tag{24}$$

with

$$\mathrm{trig} = \begin{cases} 1 & \text{if the coupling contactor is ON,} \\ 0 & \text{if the coupling contactor is OFF.} \end{cases}$$

3 Proposed synchronisation procedure

The starting/coupling procedure is based on two controls. The first one is a mechanical control at the blades level. The second control is an electrical control at the rotor windings supply voltage level. (Parameters of the generator used are given in table 1 and table 2.)

Table 1. Wind turbine characteristics.

Parameter	ρ (Kg/m^3)	G	R (m)
Value	1.22	35	13.5

Table 2. DFIG characteristics.

Parameter	P (kW)	U (V)	f (Hz)	R_s (Ω)	R_r (Ω)	L_{ss} (mH)	L'_{sr} (mH)	L_{ms} (mH)	J (Kg $\cdot$ m^2)	p
Value	300	690	50	0.0089	0.0137	12.53	12.53	12.67	100	1

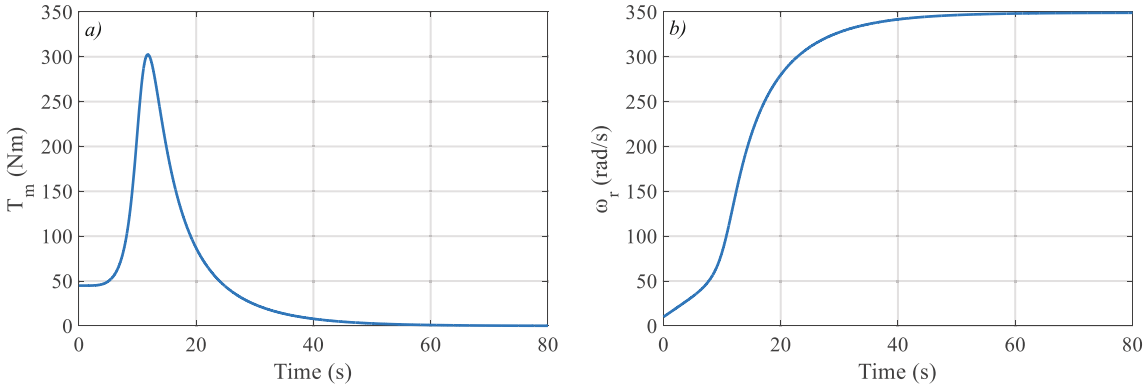

Fig. 2. Computation of mechanical equation in unloaded DFIG mode.

3.1 Mechanical control

Let a 7 m/s wind speed and a 4° pitch angle. Figures 2(a) and (b) give computing of eq. (17), respectively, for mechanical torque and rotor speed.

The idea is to let wind rotate the turbine's blades with no connection to the grid from the stator side. Dynamics of rotor shaft speed is given by fig. 2. It can be noticed that the mechanical torque returns to zero after reaching a maximum value corresponding to the operating conditions (wind speed and pitch angle). When the latter reaches zero, the rotor speed is then held at a steady state value. This criterion will be used for the generator connection to the grid.

The choice of the pitch angle is arbitrary within a given wind speed. Each pitch angle gives a different value of the rotor speed steady state (final value). This last must only remain into 70% to 130% of the synchronous angular speed, so the slip will not exceed ±30%, due to converters sizing charts [22,25]. In other words, the 4° pitch is not a unique solution for a 7 m/s wind speed.

3.2 Electrical control

As is done for synchronous machines, in unloaded operation, to each specific excitation corresponds a specific EMF. Then, there is one excitation which gives a stator EMF identical to the grid voltage. The DFIG can be coupled to the network without problems as soon as potential difference is zero between the stator and the grid. The excitation for DFIG is the rotor voltage vector, $\overline{v}_2$, which is expressed as follows:

$$\overline{v}_2 = V_r\sqrt{2}\; e^{i(2\pi f_2 t+\varphi_2)}. \tag{25}$$

There are three main factors in this voltage; a specific choice of these factors leads to a synchronization with the grid. The factors are

- f_2: Frequency of the rotor voltage.
- V_r: RMS of the rotor voltage.
- φ_2: Phase angle of the rotor voltage.

3.2.1 Frequency of the rotor voltage

The stator currents pulsation ω_s is the sum of rotor currents pulsation ω_2 and rotor angular speed ω_r. To have a synchronization between stator and grid currents pulsations, the following equation has to be respected

$$\omega_s = \omega_2 + \omega_r = \omega_1. \tag{26}$$

For this step, the rotor angular speed must be known. The most common solution gathered in the literature and put into practice by the industry to measure this value is by means of an encoder coupled to the rotor [22]. Once the ω_r steady state is reached (like the case in fig. 2(b)) and determined, the frequency of the rotor supply voltage is given by eq. (27),

$$f_2 = \frac{\omega_1 - \omega_r}{2\pi}\,. \tag{27}$$

3.2.2 RMS of the rotor voltage

The relationship between stator and rotor flux is deduced from eqs. (13) and (15):

$$\overline{\Psi}_s = \frac{M}{L_r}(\overline{\Psi}_r). \tag{28}$$

So, the expression of the stator EMF is deduced by substituting eq. (28) into eq. (12):

$$\overline{e}_s = -\frac{M}{L_r}\left(\dot{\overline{\Psi}}_r + i\omega_1\overline{\Psi}_r\right), \tag{29}$$

$$\overline{e}_s = -M\left(\dot{\overline{i}}_r + i\omega_1\overline{i}_r\right). \tag{30}$$

$\overline{i}_r$ can be given also by

$$\overline{v}_2 = (R_r + iL_r\omega_2)\overline{i}_r, \tag{31}$$

$$\overline{i}_r = \frac{\overline{v}_2}{R_r + iL_r\omega_2}. \tag{32}$$

Stator EMF is given by the following eq. (33), then its RMS by eq. (34), knowing that once the steady state is reached, $\dot{\overline{i}}_r$ disappears in eq. (30),

$$\overline{e}_s = -Mi\omega_1\frac{\overline{v}_2}{R_r + iL_r\omega_2}, \tag{33}$$

$$E_s\sqrt{2} = M\omega_1\frac{V_r\sqrt{2}}{\sqrt{{R_r}^2 + (L_r\omega_2)^2}}. \tag{34}$$

Finally, to have an equality between the stator EMF and the grid voltage V_1, the RMS of the rotor supply voltage has to respect

$$V_r = \frac{\sqrt{{R_r}^2 + (L_r\omega_2)^2}}{M\omega_1}\ V_1. \tag{35}$$

3.2.3 Phase angle of the rotor voltage

Unlike the two previous parameters, which depend only on the wind speed and the pitch angle, the phase angle depends further on the position of the rotor at the feed time ($t = 0$).

The expression of the rotor supply phase angle is determined when analysing the following eqs. (36) and (37) of the rotor supply voltage after bringing it to synchronous reference frame:

$$\overline{v}_r = V_r\sqrt{2}\ e^{i(\omega_2 t + \varphi_2)}e^{i\theta}e^{-i\omega_1 t}, \tag{36}$$

$$\overline{v}_r = V_r\sqrt{2}\ e^{i(\theta_2 + \theta - \theta_1)}, \tag{37}$$

where θ is the mechanical angle between rotor and stator, θ_2 is the angular position of $\overline{v}_2$ and θ_1 is the angular position of the grid voltage.

We can write the *d*-*q* components of the supply voltage from eq. (37) by eqs. (38) and (39):

$$V_{rd} = V_r\sqrt{2}\ \cos(\theta_2 + \theta - \theta_1), \tag{38}$$

$$V_{rq} = V_r\sqrt{2}\ \sin(\theta_2 + \theta - \theta_1). \tag{39}$$

Neglecting the voltage drop due to the rotor resistance ($R_r I_{rq} \approx 0$) and after transient state (when $\dot{\Psi}_{rq}$ becomes zero) on eqs. (14), the following equality condition of V_{rq} has to be verified:

$$V_r\sqrt{2}\sin(\theta_2 + \theta - \theta_1) = -\omega_2\Psi_{rd}. \tag{40}$$

Considering eq. (29), we can also write the "*d*" component of the rotor flux by

$$\Psi_{rd} = -V_1\sqrt{2}\frac{L_r}{M\omega_1}. \tag{41}$$

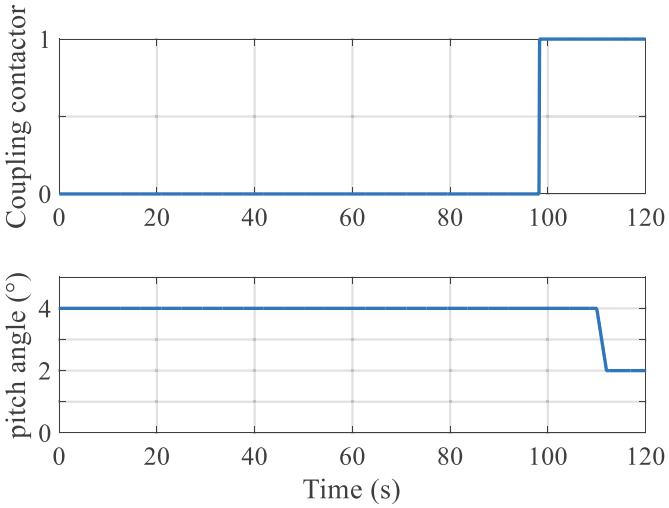

Fig. 3. Evolution of state of the coupling contactor and the pitch angle.

The position θ_2 is then deduced from eqs. (40) and (41):

$$\theta_2 = \text{asin}\left(\frac{L_r}{M}\frac{\frac{\omega_2}{\omega_1}V_1}{V_r}\right) + \theta_1 - \theta. \tag{42}$$

Finally, knowing that $\theta_2 = \omega_2 t + \varphi_2$, the phase angle is then given by

$$\varphi_2 = \theta_2 - \int \omega_2 \mathrm{d}t. \tag{43}$$

This value of phase angle given by (43) with respect to the angular position given by (42) is the key to verify the condition on eq. (40). This way, a full synchronisation between the stator and the grid is guaranteed.

3.3 Steps of the synchronisation

As soon as the blades begin rotating, as is shown in fig. 2(b), after a lap of time the rotor speed reaches a steady state where the mechanical power (*i.e.* mechanical torque) is zero (fig. 2(a)).

The rotor can be supplied, from this moment, with a voltage given by eq. (25) with values corresponding to eqs. (27), (35) and (43).

In the case of a pre-studied system and a constant wind speed, the rotor can be supplied from the beginning. Otherwise, the system has to be let until ω_r (rotor angular speed) reach its steady state and measure it, as f_2, V_r and φ_2 depend only on the rotor speed.

Then, the coupling contactor between the stator and the grid can be switched ON. The coupling is safe and smooth as the potential difference between stator and grid is zero; also, there is no power flow as the mechanical power is zero.

Finally, blades control is given back to the pitch control system responsible for maximum power extraction from the wind or power capture limitation for higher wind speeds.

4 Simulation results and discussion

Figure 3 gives the coupling instant and variation of the pitch angle as a simulation condition.

Let a 7 m/s wind speed, and J was taken as $10\,\text{Kg}\cdot\text{m}^2$ instead of $100\,\text{Kg}\cdot\text{m}^2$ to accelerate simulation. ω_r took about 85 s to reach its steady state. The rotor is supplied at this moment. The system detects full synchronization with grid and connects the generator at 98.3 s. At 110 s, the blades pitch position is moved from 4° to 2°. From 112 s, the full power extracted from the wind is fed to the grid.

From fig. 4(a), 349.11 rad/s is the rotor speed before coupling, this gives a −34.95 rad/s pulsation for the rotor supply voltage (*i.e.* a frequency of −5.56 Hz). The negative sign on f_2 corresponds to an over-synchronous operation of the DFIG.

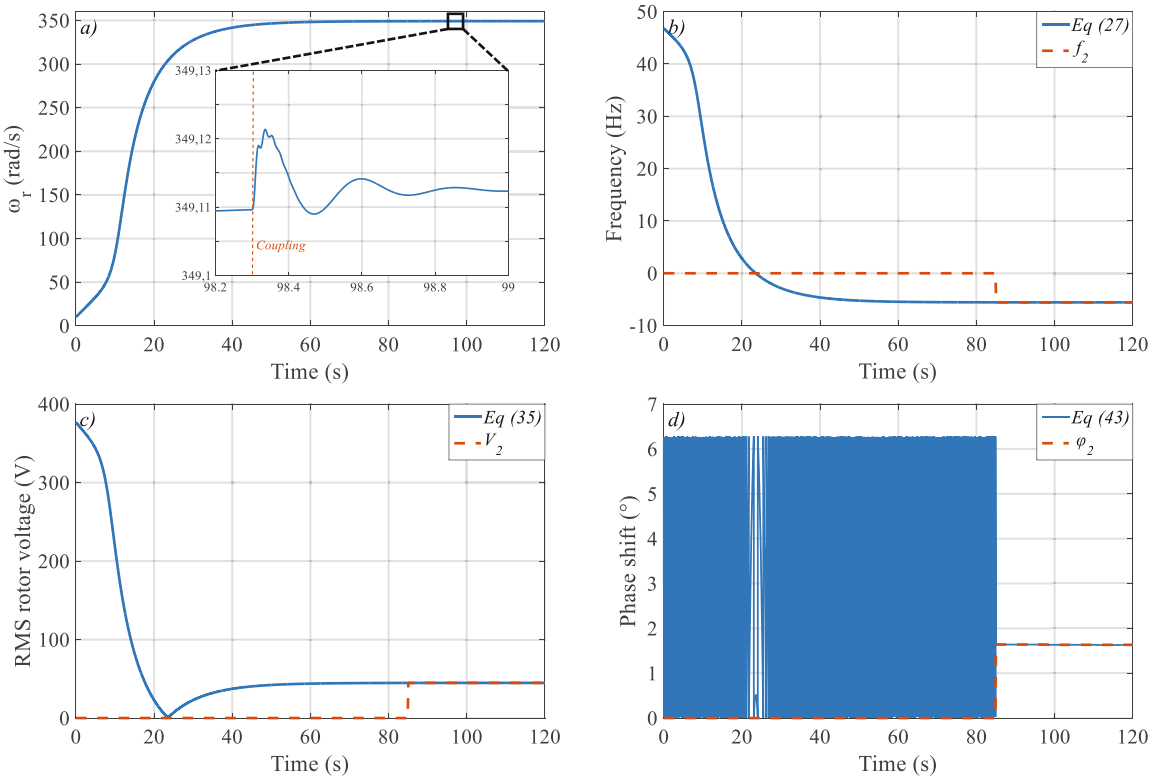

Fig. 4. Rotor voltage supply parameters according to the rotor speed.

Figures 4(b), (c) and (d) give, respectively, frequency, RMS and phase angle of the rotor supply voltage. The blue curves (continuous lines) give computation of equations of the rotor voltage parameters from the beginning of simulation. The second curve (dashed lines) in the same figure gives actual rotor control signal, which was chosen to be supplied at simulation time 85 seconds.

The transient state for the rotor speed during the grid coupling is barely noticeable (variation amplitude is about 0.01 rad/s), which confirms the stability of the proposed procedure as the rotor was not subject of mechanical stress. The proposed technique showed its damping capability compared to the results given in [20].

As soon as the rotor is supplied with the parameters in fig. 4, the stator EMF appears and, after a small transient state, it converges to the grid voltage value. The amplitude of the stator EMF vector is given in fig. 5(a). A zoom of this figure during grid connection is given in fig. 6(a).

In fig. 5(b) the variation of the current is stable and the transient during the coupling has not exceeded 1% of the rated value and converges in very short time to normal operation. This coupling procedure shows better results than the ones given in the available literature so far [18,19]. Also, the proposed DFIG's model allowed assessment of the machine's behaviour along the coupling process. None of the previous works proposed such modelling for the DFIG in its different states and none of them showed state of these variables during connection.

The modelling and the behaviour assessment of the machine especially in unloaded conditions proved that functioning of the DFIG is close enough to a wound rotor synchronous machine except for an AC excitation (inductor) instead of a DC one. Unlike ordinary asynchronous machines, the DFIG is capable of producing an EMF even without stator connection. This criterion was used to enhance DFIG-Grid connection where the inductor was fed in a precise way to have the full synchronization.

Connection of the machine at zero mechanical power showed its damping efficiency where all variables affecting the safety of the machine were stable and converged in a very short time after transient state.

As soon as the pitch angle is decreased, the mechanical torque increased according to mechanical equations of the turbine (1) to (5). The mechanical torque rise causes, accordingly, an increase in the electromagnetic torque (explained by the mechanical equation (11)), which implies the beginning of the current feed.

Figures 5(c), (d) and (e) represent, respectively, the generator active power, reactive power and turbine mechanical power. The variation on these curves is according to the current evolution.

The dead time between the coupling and the beginning of power injection is a procedure choice for the simulation and is not imperative. It shows that the machine, meanwhile, is connected to the grid without power flow on both sides since the potential difference is zero between the grid and the stator EMF. This proves the stability of the procedure

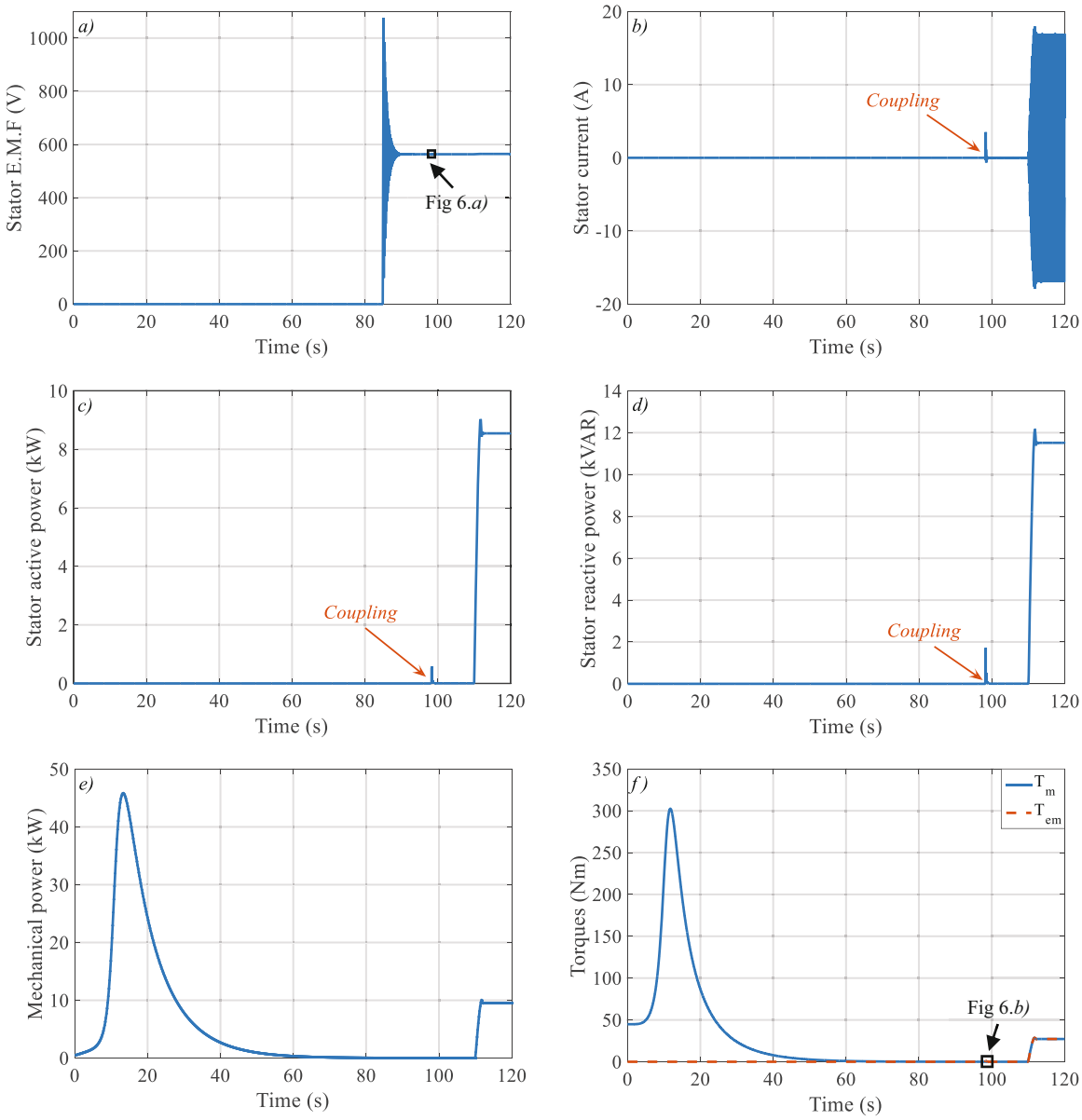

Fig. 5. Proposed starting/coupling procedure consequences on system outputs.

as the machine finished connection to the grid, the power injection did not start and yet, there no harm to the machine or the grid after connection.

A zoom of the torques figure (fig. 5(f)) during grid connection is given in fig. 6(b).

Disturbance during coupling is not remarkable for the stator EMF and the electromagnetic torque. Variation is about 0.015 V for stator EMF and 10 Nm for electromagnetic torque (representing about 1% of the nominal torque) which does not affect the generator. The negative variation of the electromagnetic torque is transient state during this brief lap of time. This functioning is permitted as long as the amplitude and duration are limited.

Figure 7 gives the curve "Mechanical torque – speed", whose synchronization process and the variation of the operating point in this plan during this procedure are explained further.

Point "A" is the first break point of the system as the starting point. The wind turbine is decoupled from the grid and the blades are standstill. Once the brakes are released and under a certain wind speed, the operating point moves to the second break point "B" according to the lower curve (in blue, corresponds to the 4° pitch). The system is currently in "B", the rotor is supplied with the proper voltage at simulation time 85 s. The grid coupling contactor is switched on by detection of the synchronism at 98.3 s and the system is still in "B". At 110 s, the pitch angle is reduced from 4° to 2°. The system then moves to point "C" in the upper curve (in red) at a constant speed. The injection of power into the grid starts as soon as the system leaves the point "B" to the third break point "C". From

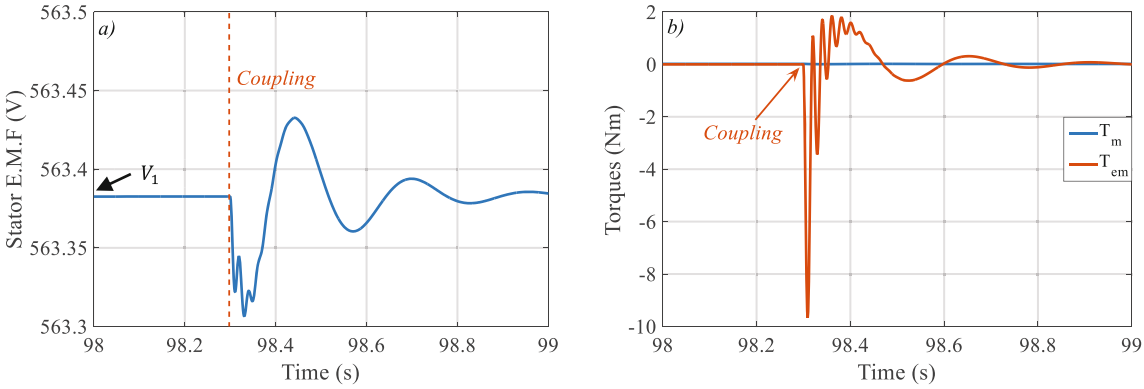

Fig. 6. Zoom of the stator EMF and the torques figures during connection.

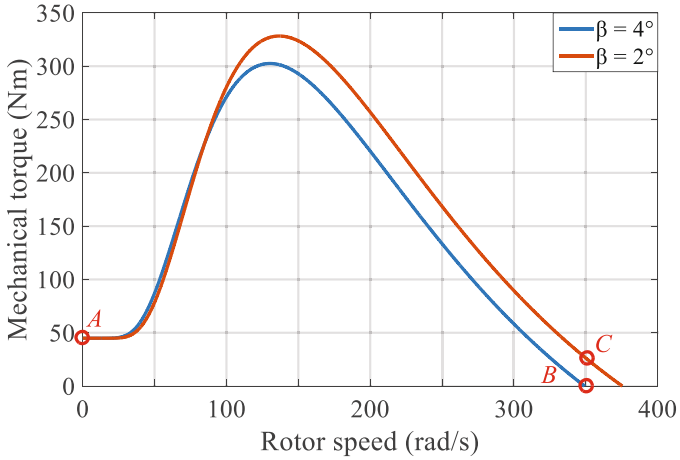

Fig. 7. Critical operation break-points.

this operation point, the user can apply any type of possible control on the machine as it is coupled to the grid and stable. Due to the non-linearity of the system model, usually, controls applied on DFIG wind systems are non-linear controls (sliding mode control, backstepping control, etc.) based on stator flux orientation as this control technique allows a decoupled control of both active and reactive powers [11,22,26].

5 Conclusions

An improved and practical starting/coupling procedure for a DFIG based WTG was detailed in this work based on specific excitation inspired from what it is formerly done for synchronous generators. In fact, improvement involves stability of the machine during synchronization. As the coupling process is done at no mechanical power and no potential difference between the stator and grid voltages, no harmful operations were recorded during the connection.

A study of the system allowed its modelling for its different states, a loaded DFIG model, an unloaded DFIG model and finally a VSS model combining the two states of the machine. Simulation results showed clearly that the proposed model reproduces well dynamics of the DFIG all over the coupling process. Particularly, during coupling to the grid (under model switching), the proposed procedure showed its efficiency, smoothness and safety, where system outputs variations do not exceed 1% of nominal values (no currents or torque surges).

The results mean physically that the generator was not subject of harmful operations, *i.e.* no mechanical stress on the rotor shaft nor perturbation in grid currents. The other advantage is that the proposed procedure is done regardless the control that will be applied on the generator and set by the user once coupled to the grid.

Finally, since synchronous generators are deeply investigated, we will search for further similarities and look if known and robustness-proved controls applied on these machines are valid also for DFIGs. In this case, DFIG's can be further exploited for more wind generation integration efficiency. Future works will involve more post-coupling issues.

The authors of this work would like to thank the University of Sfax, Tunisia and all the crew of the research unit CMERP for providing the facilities and research grant to achieve this research, and greatly thank the reviewers for taking time to evaluate this work.

Nomenclature

P:	DFIG nominal power	L_r:	$L'_{sr} + L_{mr}$
U:	DFIG nominal line to line voltage	L_{ss}:	Inductance of a stator phase
f_1:	Grid frequency	L'_{sr}:	Inductance of a rotor phase
p:	Number of pole pairs	L_{ms}:	Magnetizing inductance of stator phase
J:	Inertia of the rotor shaft	L_{mr}:	$L_{ms} \times M$
$\overline{v}_s$:	Stator voltage	M:	Maximum coefficient of mutual induction
$\overline{v}_r$:	Rotor voltage in the synchronous frame	$\overline{i}_s$:	Stator current
$\overline{v}_1$:	Grid voltage	$\overline{i}_r$:	Rotor current
ω_1:	Electric angular speed of the grid	$\overline{\Psi}_s$:	Stator flux
ω_2:	Electric angular speed for rotor windings	$\overline{\Psi}_r$:	Rotor flux
ω_r:	Angular speed of the rotor	R_s:	Resistance of a stator phase
L_s:	$L_{ss} + L_{ms}$	R_r:	Resistance of a rotor phase

References

1. *Renewables 2017 Global Status Report*, accessed Sep 2017, http://www.ren21.net/gsr-2017/.
2. Ming Cheng, Ying Zhu, Energy Convers. Manag. **88**, 332 (2014).
3. Alshehri Abdullah, Afef Fekih, *An Overview of the Current State of Wind Energy Technology Development in the US*, in *2013 IEEE Green Technologies Conference, 4-5 April 2013, Denver, CO, USA* (IEEE, 2013) pp. 120–126, https://doi.org/10.1109/GreenTech.2013.26.
4. *Wind Report, Global Wind Energy Council (GWEC), 2016*, accessed on September 2016, available on-line at the following link: http://gwec.net/publications/global-wind-report-2/global-wind-report-2016/.
5. V.N. Pande, U.M. Mate, Shailaja Kurode, Electr. Power Syst. Res. **100**, 73 (2013).
6. S. Abdeddaim, A. Betka, Electr. Power Energy Syst. **49**, 234 (2013).
7. Arjang Yousefi-Talouki, Edris Pouresmaeil, Bo Nørregaard Jørgensen, Electr. Power Energy Syst. **63**, 600 (2014).
8. F. Akela, T. Ghennam, E.M. Berkouk, M. Laour, Energy Convers. Manag. **78**, 584 (2014).
9. W. Yi, X. Lie, IEEE Trans. Power Deliv. **25**, 367 (2010).
10. S. Lei, H. Jiabing, IEEE Trans. Energy Convers. **27**, 362 (2012).
11. M.I. Martinez, G. Tapia, A. Susperregui, H. Camblong, IEEE Trans. Energy Convers. **27**, 328 (2012).
12. G. Abad, M.A. Rodriguez, G. Iwanski, J. Poza, IEEE Trans. Power Electron. **25**, 442 (2010).
13. M. Kenan Döşoğlu, Ali Öztürk, Adv. Eng. Softw. **45**, 292 (2012).
14. Ali Öztürk, Kenan Döşoğlu, *Investigation of the control voltage and reactive power in wind farm load bus by STATCOM and SVC*, in *International Conference on Electrical and Electronics Engineering - ELECO 2009, 5–8 Nov. 2009, Bursa, Turkey*, (2009) pp. I-60-I-64, https://doi.org/10.1109/ELECO.2009.5355356.
15. M. Kenan Döşoğlu, Int. J. Electr. Power Energy Syst. **83**, 251 (2016).
16. M. Kenan Döşoğlu, Int. J. Electr. Power Energy Syst. **78**, 655 (2016).
17. M. Kenan Döşoğlu, Ayşen Basa Arsoy, Int. J. Electr. Power Energy Syst. **78**, 414 (2016).
18. R. Pena, J.C. Clare, G.M. Asher, IEEE Proc. Electr. Power Appl. **143**, 231 (1996).
19. S.A. Gomez, J.L.R. Amenedo, *Grid synchronisation of doubly fed induction generators using direct torque control*, in *IEEE 2002 28th Annual Conference of the Industrial Electronics Society, IECON 02, 5–8 Nov. 2002, Sevilla, Spain*, Vol. **4**, pp. 3338-3343, https://doi.org/10.1109/IEMDC.2007.382704.
20. Ahmed G. Abo-Khalil, Renew. Energy **44**, 193 (2012).
21. S. Kammoun, A. Marrekchi, S. Sallem, M. Kammoun, Int. J. Mod. Nonlinear Theory Appl. **3**, 77 (2014).
22. Gonzalo Abad, Jesús López, Miguel A. Rodríguez, Luis Marroyo, Grzegorz Iwanski, *Doubly fed induction machine: modeling and control for wind energy generation* (IEEE Press, John Wiley & Sons, Inc., New Jersey, 2011) https://doi.org/10.1002/9781118104965.
23. Hüseyin Altun, Sedat Sünter, Electr. Eng. **95**, 157 (2013).
24. Rishabh Dev Shukla, Ramesh Kumar Tripathi, Renew. Sustain. Energy Rev. **37**, 69 (2014).
25. Eduard Muljadi, Mohit Singh, Vahan Gevorgian, *Doubly Fed Induction Generator in an Offshore Wind Power Plant Operated at Rated V/Hz*, in *IEEE Energy Conversion Congress and Exhibition Raleigh, North Carolina September 15-20, Conference Paper NREL/CP-5500-55573, June 2012* (2012) https://doi.org/10.1109/TIA.2013.2261043.
26. A. Mechter, K. Kemih, M. Ghanes, *Backstepping control of a wind turbine for low wind speeds*, Nonlinear Dyn., (2016) https://doi.org/10.1007/s11071-016-2655-y.